Available online at www.sciencedirect.com
ScienceDirect
Journal of Sound and Vibration 317 (2008) 608–624
JOURNAL OF SOUND AND VIBRATION
www.elsevier.com/locate/jsvi

Simulation of spur gear dynamics and estimation of fault growth ☆

Siyan Wu, Ming J. Zuo*, Anand Parey

Department of Mechanical Engineering, University of Alberta, Edmonton T6G2G8, Canada

Received 31 May 2007; received in revised form 2 January 2008; accepted 24 March 2008
Handling Editor: S. Bolton
Available online 9 May 2008

Abstract

In this paper, the effects of tooth crack on the vibration response of a one-stage gearbox with spur gears are studied. The growth in a tooth crack is reflected in the total mesh stiffness of the gear system. A lumped parameter model is used to simulate the vibration response of the pair of meshing gears. Several statistical indicators reported in the literature are used to reflect the change in the vibration response caused by the tooth crack. The performance of these indicators are compared. Their pros and cons are outlined.

1. Introduction

Gearboxes are among the most important mechanisms in industrial machinery, automotive applications, and our daily lives. They are widely used to transmit power and produce high rotational speed changes and/or change the direction of motion. Because of their growing use in modern technology, gearbox health monitoring and early fault detection has become the subject of intensive investigation and research [1].

A great deal of research has been undertaken to study the dynamic modelling of spur gears. Kasuba and Evans [2] used a digitization approach to calculate gear mesh stiffness. Yang and Lin [3] used the so-called potential energy method to express the total mesh stiffness of a pair of meshing gears as a function of the rotation angle of the gear. Their model was further refined by Tian [4] by taking the shear mesh stiffness into consideration. Bartelmus [5] applied mathematical modelling and computer simulation to gearbox dynamic examinations. Both torsional and lateral vibrations were included in his study of a one-stage spur gearbox system. An eight degrees of freedom model including friction was also given in Ref. [5]. Tammigana et al. [6], Vedmar and Anderson [7], Kartik and Houser [8], Velex and Ajmi [9], and He et al. [10] have recently reported more sophisticated dynamic models of spur and/or helical gears including various degrees of freedom, various excitation factors such as gear transmission errors, and various nonlinearities such as variable mesh stiffness,

☆A shorter version of this paper was presented at the Second World Congress on Engineering Asset Management in Harrogate, UK, June 11–14, 2007.

*Corresponding author. Tel.: +1 780 492 4466; fax: +1 780 492 2200.
E-mail address: ming.zuo@ualberta.ca (M.J. Zuo).

0022-460X/$ - see front matter © 2008 Elsevier Ltd. All rights reserved.
doi:10.1016/j.jsv.2008.03.038

mesh damping, and gear geometrical errors. These models provide more realistic representations of the dynamic behavior of the meshing gears. However, they have not considered the effects of mechanical damages on the dynamic response of the system.

These various gear dynamic models may provide useful information for fault detection. Vibration-based time domain, frequency domain, and time-frequency domain analyses constitute the most powerful tools available for fault detection of rotating machinery. One traditional technique is based on statistical measurements of the vibration signal. The simplest indicators include peak, root mean square (rms), and crest factor (CF). Kurtosis is a widely used higher order statistic, and its successful use has been reported for bearing condition monitoring [11]. Fault Growth Parameter (FGP) and its revised version FGP1 are two other newly proposed indicators which have been proved to provide a clear way to track the development of cracks (or spalls) in gear teeth [12].

The scope of this paper is limited to a spur gear pair. This paper reports the results developed by Wu [13] and a simpler version of this paper is reported in Wu and Zuo [14]. Computer simulation is used to study the effects of tooth crack on the vibration response of a one-stage gearbox with spur gears. A tooth root crack with a range of sizes is introduced to one of the pinion teeth, and the corresponding vibration responses are simulated. Different statistic indicators are applied to detect the tooth damage. The performance of these indicators is investigated. Since we are focusing on the effects of a growing crack on the vibration response of the meshing gears, we have ignored the effects of manufacturing errors in the gears, the frictions between the gear teeth, and other practical phenomena such as backlash.

2. Modelling of gear mesh stiffness when a tooth is cracked

The gear mesh stiffness model described in this study was based on the work by Yang and Lin [3] in 1987. They used the potential energy method to analytically model the effective mesh stiffness. The total potential energy stored in the meshing gear system was assumed to include three components: Hertzian energy, bending energy, and axial compressive energy. This model was refined by Tian [4] in 2004 in which shear energy was taken into account as well. Thus, for the single-tooth-pair meshing duration, the total effective mesh stiffness can be expressed as [4]

$$k_t = \frac{1}{1/k_h + 1/k_{b1} + 1/k_{s1} + 1/k_{a1} + 1/k_{b2} + 1/k_{s2} + 1/k_{a2}}, \tag{1}$$

where k_h, k_b, k_s, and k_a represent the Hertzian, bending, shear, and axial compressive mesh stiffness, respectively. For the double-tooth-pair meshing duration, the total effective mesh stiffness is the sum of the two pairs' stiffnesses, which is shown as [4]

$$k_t = \sum_{i=1}^{2} \frac{1}{1/k_{h,i} + 1/k_{b1,i} + 1/k_{s1,i} + 1/k_{a1,i} + 1/k_{b2,i} + 1/k_{s2,i} + 1/k_{a2,i}}, \tag{2}$$

where $i = 1$ represents the first pair of meshing teeth and $i = 2$ represents the second. The derivations of these two equations are given in Tian [4]. Calculation of each of the components in these two equations when there are no cracks in any gear is given in Refs. [3,4,15], where Ref. [15] is a shorter version of Ref. [4]. The expressions of these components when cracks are introduced will be provided later in this paper.

For typical gear parameters given in Table 1, we wrote simple Matlab programs and obtained numerical values of the total effective mesh stiffness as a function of the gear rotation angle. This total effective mesh stiffness within one shaft period of the gear is plotted in Fig. 1. Fig. 1 represents the total meshing stiffness of the pair of gears when the gear teeth are perfect (that is, have no cracks).

On crack development in a gear, Refs. [16–19] consider that a crack is developing at the root of a single tooth of the pinion. A tooth root crack typically starts at the point of the largest stress in the material. In Ref. [20], a computational model which applies the principles of linear elastic fracture mechanics is used to simulate gear tooth root crack propagation. Based on the computational results, the crack propagation path shows a slight curve extending from the tooth root as shown in the left side of Fig. 2 [20]. Lewicki [21] also indicates that crack propagation paths are smooth, continuous, and in most cases, rather straight with only a

Table 1
Main parameters of the gear and pinion [15]

Young's modulus	$E = 2.068 \times 10^{11}$ Pa
Poisson's ratio	$v = 0.3$
Pressure angle	20°
Diametral pitch	$P = 0.2032\,\mathrm{m}^{-1}$
Width of teeth	$L = 0.16$ m
Number of teeth on pinion	$N_1 = 19$
Number of teeth on gear	$N_2 = 48$

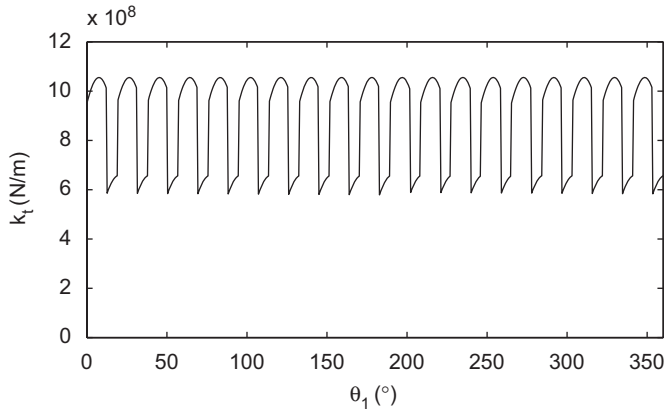

Fig. 1. The total effective mesh stiffness, k_t vs. the pinion's angular displacement, θ_1, within one shaft period, when the gear teeth are perfect.

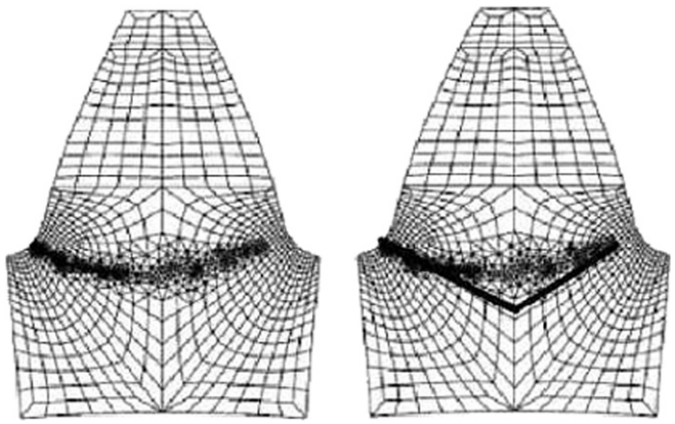

Fig. 2. Assumed crack propagation path.

slight curvature. He has also studied the effects of rim and web thickness on crack propagation path and showed that different paths exist.

In this paper, based on the results shown in Ref. [20], we further simplify the crack model. We will consider the crack path to be a straight line as shown in the right side of Fig. 2. The crack starts at the root of the pinion and then proceeds as shown in Fig. 2. Further referring to Figs. 3–6, the intersection angle, υ, between the crack and the central line of the tooth is set at a constant 45°. The crack length, q_1, grows from zero with an increment size of $\Delta q_1 = 0.1$ mm until the crack reaches the tooth's central line. At that point, q_1, reaches its maximum value of 3.9 mm. After that, the crack then changes direction to q_2 (see Fig. 5), which is assumed to be exactly symmetric around the tooth's central line. Theoretically, the maximum length of q_2 should be the

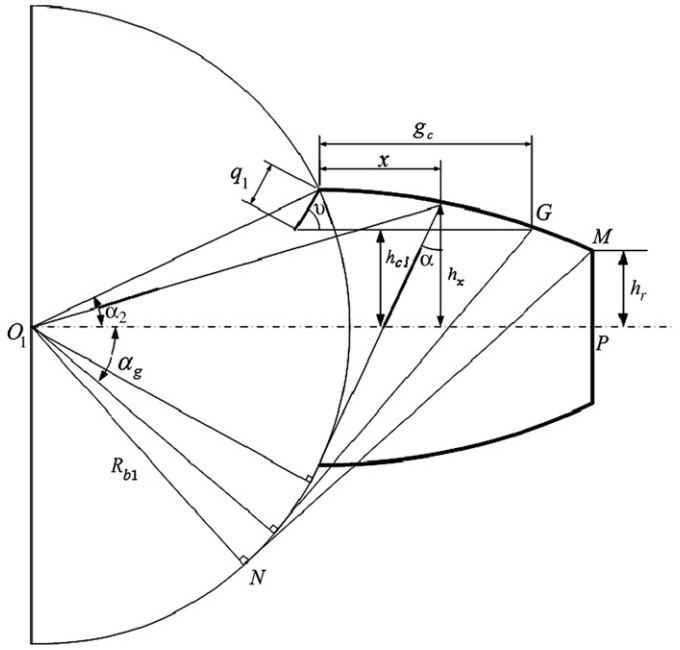

Fig. 3. The cracked tooth model for case 1.

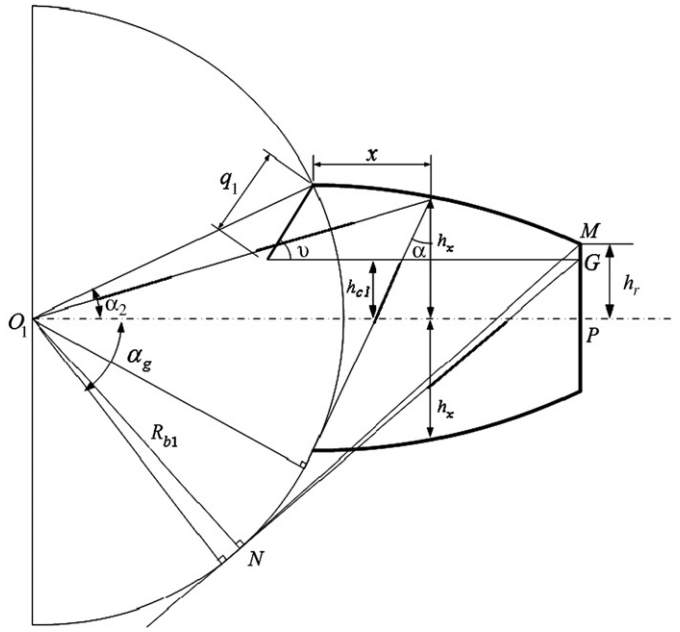

Fig. 4. The cracked tooth model for case 2.

same as q_1, however, the tooth is expected to suffer sudden breakage before the crack runs through the whole tooth. Thus the maximum length of q_2 is assumed to be 60% of $q_{1\max}$ and the increment size, Δq_2, is also 0.1 mm. In later reference of the crack growth, we will use a relative length. The highest crack level will be $3.9 + 60\% \times 3.9 = 6.24$ mm, or 80% ($= 6.24/7.8$) of the theoretical total length of the full through crack.

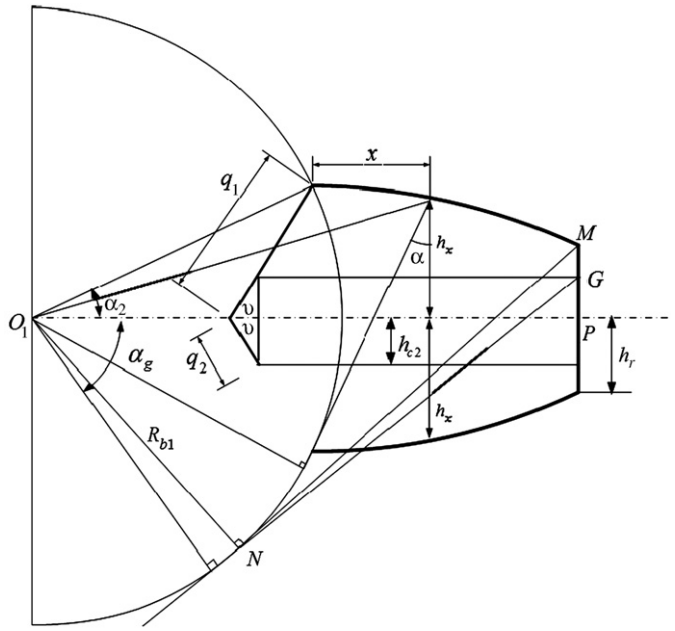

Fig. 5. The cracked tooth model for case 3.

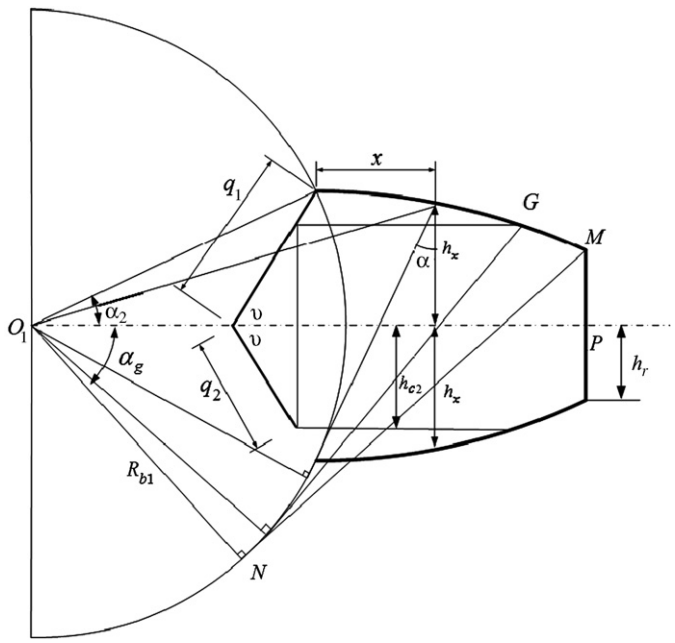

Fig. 6. The cracked tooth model for case 4.

With the crack introduced as described above, we need to calculate all components of the total mesh stiffness, that is, Hertzian stiffness, axial compressive stiffness, bending stiffness, and shear stiffness. Based on the work documented in Ref. [15], the Hertzian and axial compressive stiffnesses remain the same when a crack is introduced. However, the bending and shear stiffnesses will change due to the appearance of the crack, and their derivation are provided under each of the following four cases.

Case 1 Tian [4]: When $h_{c1} \geqslant h_r$ & $\alpha_1 > \alpha_g$, where $\alpha_1 = 90^\circ -$ (pressure angle).

The potential energy stored in a meshing gear tooth can be calculated by

$$U_b = \int_0^d \frac{M^2}{2EI_x}\,\mathrm{d}x = \int_0^d \frac{[F_b(d-x) - F_a h]^2}{2EI_x}\,\mathrm{d}x, \tag{3}$$

$$U_s = \int_0^d \frac{1.2F_b^2}{2GA_x}\,\mathrm{d}x = \int_0^d \frac{[1.2F\cos\alpha_1]^2}{2GA_x}\,\mathrm{d}x, \tag{4}$$

where I_x and A_x represent the area moment of inertia and area of the section where the distance from the tooth's root is x, and G represents the shear modulus. They can be obtained by

$$I_x = \begin{cases} \dfrac{1}{12}(h_{c1}+h_x)^3 L & \text{if } x \leqslant g_c, \\ \dfrac{1}{12}(2h_x)^3 L & \text{if } x > g_c, \end{cases} \tag{5}$$

$$A_x = \begin{cases} (h_{c1}+h_x)L & \text{if } x \leqslant g_c, \\ 2h_x L & \text{if } x > g_c, \end{cases} \tag{6}$$

$$G = \frac{E}{2(1+v)}, \tag{7}$$

where h_x represents the distance between the point on the tooth's curve and the tooth's central line where the horizontal distance from the tooth's root is x.

The bending mesh stiffness of the cracked tooth is

$$\begin{aligned} \frac{1}{k_{b_{\text{crack}}}} = & \int_{-\alpha_g}^{\alpha_2} \frac{12\{1+\cos\alpha_1[(\alpha_2-\alpha)\sin\alpha-\cos\alpha]\}^2(\alpha_2-\alpha)\cos\alpha}{EL[\sin\alpha_2-(q_1/R_{b1})\sin\upsilon+\sin\alpha+(\alpha_2-\alpha)\cos\alpha]^3}\,\mathrm{d}\alpha \\ & + \int_{-\alpha_1}^{-\alpha_g} \frac{3\{1+\cos\alpha_1[(\alpha_2-\alpha)\sin\alpha-\cos\alpha]\}^2(\alpha_2-\alpha)\cos\alpha}{2EL[\sin\alpha+(\alpha_2-\alpha)\cos\alpha]^3}\,\mathrm{d}\alpha \end{aligned} \tag{8}$$

and the shear mesh stiffness of the cracked tooth is

$$\begin{aligned} \frac{1}{k_{s_{\text{crack}}}} = & \int_{-\alpha_g}^{\alpha_2} \frac{2.4(1+v)(\alpha_2-\alpha)\cos\alpha(\cos\alpha_1)^2}{EL[\sin\alpha_2-(q_1/R_{b1})\sin\upsilon+\sin\alpha+(\alpha_2-\alpha)\cos\alpha]}\,\mathrm{d}\alpha \\ & + \int_{-\alpha_1}^{-\alpha_g} \frac{1.2(1+v)(\alpha_2-\alpha)\cos\alpha(\cos\alpha)^2}{EL[\sin\alpha_2-(q_1/R_{b1})\sin\upsilon+\sin\alpha+(\alpha_2-\alpha)\cos\alpha]}\,\mathrm{d}\alpha. \end{aligned} \tag{9}$$

Case 2 Tian [4]: When $h_{c1} < h_r$ or when $h_{c1} \geqslant h_r$ & $\alpha_1 \leqslant \alpha_g$.

The bending mesh stiffness of the cracked tooth is

$$\frac{1}{k_{b_{\text{crack}}}} = \int_{-\alpha_1}^{\alpha_2} \frac{12\{1+\cos\alpha_1[(\alpha_2-\alpha)\sin\alpha-\cos\alpha]\}^2(\alpha_2-\alpha)\cos\alpha}{EL[\sin\alpha_2-(q_1/R_{b1})\sin\upsilon+\sin\alpha+(\alpha_2-\alpha)\cos\alpha]^3}\,\mathrm{d}\alpha \tag{10}$$

and the shear mesh stiffness of the cracked tooth is

$$\frac{1}{k_{s_{\text{crack}}}} = \int_{-\alpha_1}^{\alpha_2} \frac{2.4(1+v)(\alpha_2-\alpha)\cos\alpha(\cos\alpha_1)^2}{EL[\sin\alpha_2-(q_1/R_{b1})\sin\upsilon+\sin\alpha+(\alpha_2-\alpha)\cos\alpha]}\,\mathrm{d}\alpha. \tag{11}$$

Case 3: When $h_{c1} < h_r$ or when $h_{c1} \geqslant h_r$ & $\alpha_1 \leqslant \alpha_g$.

This case was not covered in Ref. [4]. The bending mesh stiffness of the cracked tooth is

$$\frac{1}{k_{b_{\text{crack}}}} = \int_{-\alpha_1}^{\alpha_2} \frac{12\{1+\cos\alpha_1[(\alpha_2-\alpha)\sin\alpha-\cos\alpha]\}^2(\alpha_2-\alpha)\cos\alpha}{EL[\sin\alpha-(q_2/R_{b1})\sin\upsilon+(\alpha_2-\alpha)\cos\alpha]^3}\,\mathrm{d}\alpha \tag{12}$$

and the shear mesh stiffness of the cracked tooth is

$$\frac{1}{k_{s_{\text{crack}}}} = \int_{-\alpha_1}^{\alpha_2} \frac{2.4(1+v)(\alpha_2-\alpha)\cos\alpha(\cos\alpha_1)^2}{EL[\sin\alpha-(q_2/R_{b1})\sin\upsilon+(\alpha_2-\alpha)\cos\alpha]}\,\mathrm{d}\alpha. \tag{13}$$

Case 4: When $h_{c2} \geqslant h_r$ & $\alpha_1 > \alpha_g$.

This case was not covered in Ref. [4] either. We have found the bending mesh stiffness of the cracked tooth to be

$$\frac{1}{k_{b_{\text{crack}}}} = \int_{-\alpha_g}^{\alpha_2} \frac{12\{1+\cos\alpha_1[(\alpha_2-\alpha)\sin\alpha-\cos\alpha]\}^2(\alpha_2-\alpha)\cos\alpha}{EL[\sin\alpha-(q_2/R_{b1})\sin\upsilon+(\alpha_2-\alpha)\cos\alpha]^3}\,\mathrm{d}\alpha \tag{14}$$

Table 2
A sample of different crack lengths

Crack size	Belonging to
$q_1 = 1.4$ mm	Case 1
$q_1 = 3.1$ mm	Case 2
$q_1 = 3.9$ mm, $q_2 = 1.1$ mm	Case 3
$q_1 = 3.9$ mm, $q_2 = 2.4$ mm	Case 4

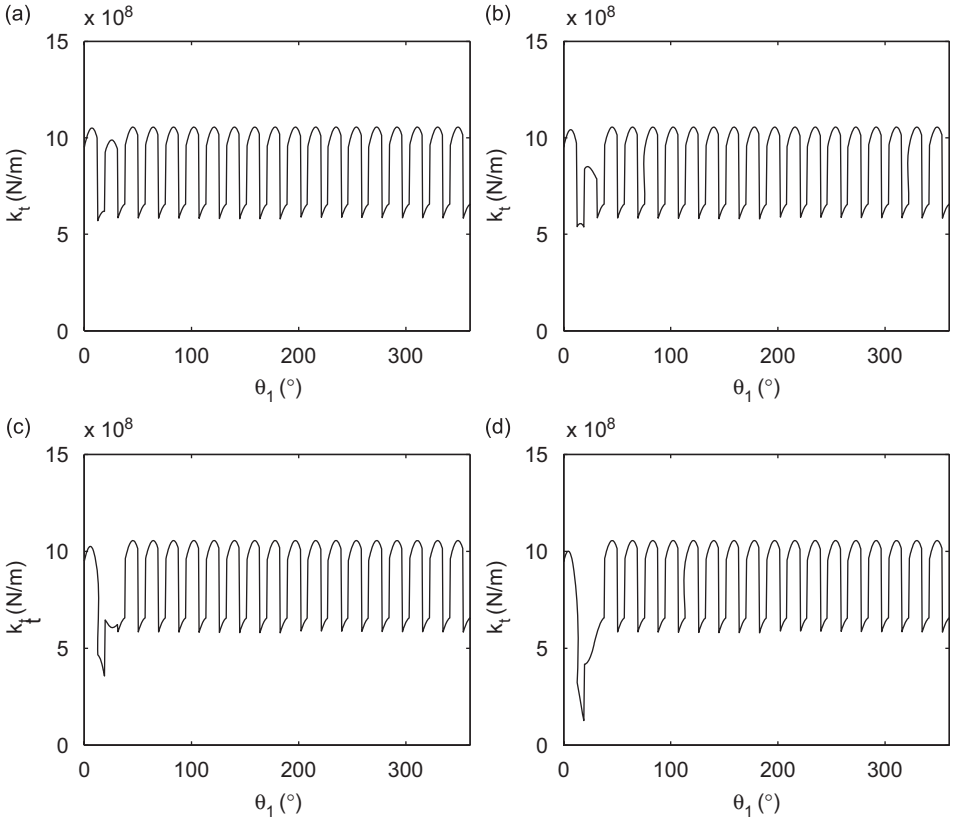

Fig. 7. The total mesh stiffness, k_t, at different crack levels: (a) Case 1: $q_1 = 1.4$ mm, (b) Case 2: $q_1 = 3.1$ mm, (c) Case 3: $q_1 = 3.9$ mm, $q_2 = 1.1$ mm, (d) Case 4: $q_1 = 3.9$ mm, $q_2 = 2.4$ mm.

and the shear mesh stiffness of the cracked tooth is

$$\frac{1}{k_{s_{\text{crack}}}} = \int_{-\alpha_g}^{\alpha_2} \frac{2.4(1+v)(\alpha_2-\alpha)\cos\alpha(\cos\alpha_1)^2}{EL[\sin\alpha-(q_2/R_{b1})\sin\upsilon+(\alpha_2-\alpha)\cos\alpha]}\,\mathrm{d}\alpha. \tag{15}$$

With the expressions of the components of the total mesh stiffness provided above, we are able to find the total mesh stiffness value given each shaft rotation angle and each crack size. For a pair of standard steel involute spur teeth whose main parameters are given in Table 1, take four specific crack sizes given in Table 2 as an example. These selected crack sizes cover all the four cases classified in the above derivations. The total mesh stiffness under each of the four crack sizes has been calculated as a function of the shaft rotation angle and plotted in Fig. 7. From Fig. 7, it can be observed that as the size of the crack grows, the total mesh stiffness when the cracked tooth is in meshing becomes much lower. This is important information for fault detection and assessment.

3. Dynamic simulation of gearbox vibration response

We will adopt the mathematical model with torsional and lateral vibration reported by Bartelmus [5] in 2001. The model of a one stage gearbox system is given in Fig. 8. It is a two-parameter (stiffness and damping) model with torsional and lateral vibration, which means that it includes both the linear and rotational equations of the system's motion. This model represents a system with six degrees of freedom, which is driven by electric motor moment, M_1, and loaded with external moment, M_2. This model is simple enough to enable to focus on the effects of crack growth on the vibration response of the system. Thus, in this paper, we have

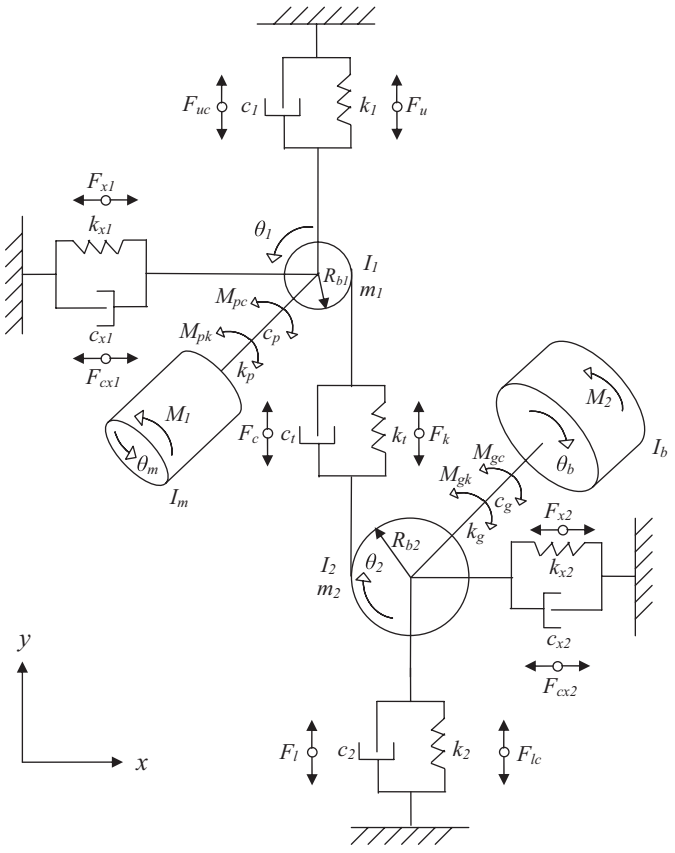

Fig. 8. A one stage gearbox system [5].

assumed that all gears are perfectly mounted rigid bodies with ideal geometries. Inter-tooth friction is ignored here for simplicity. The following notation is used in this study:

(1) F_k/F_c: stiffness/damping inter-tooth force
(2) F_u/F_{uc}: internal stiffness/damping force of input bearing
(3) F_l/F_{lc}: internal stiffness/damping force of output bearing
(4) M_{pk}/M_{pc}: stiffness/damping moment of input couplings
(5) M_{gk}/M_{gc}: stiffness/damping moment of output couplings
(6) k_t: total mesh stiffness
(7) c_t: mesh damping coefficient
(8) I_m/I_b: mass moment of inertia of motor/load
(9) I_1/I_2: mass moment of inertia of pinion/gear
(10) M_1: input motor torque
(11) M_2: output torque from load
(12) m_1/m_2: mass of the pinion/gear
(13) R_{b1}/R_{b2}: base circle radius of pinion/gear
(14) R_{O1}/R_{O2}: outside circle radius of pinion/gear
(15) k_p/k_g: torsional stiffness of input/output flexible coupling
(16) c_p/c_g: damping coefficient of input/output flexible coupling
(17) k_1/k_2: vertical radial stiffness of input/output bearings
(18) c_1/c_2: vertical radial viscous damping coefficient of input/output bearings
(19) y_1/y_2: linear displacement of pinion/gear in the y direction
(20) θ_m/θ_b: angular displacement of motor/load
(21) θ_1/θ_2: angular displacement of pinion/gear

Because friction is ignored, the vibration in the x direction is free response and will disappear due to inherent damping. In this paper, we focus only on the motion in the y direction. Based on Bartelmus [5], the vertical motion (in the y direction) equations of the pinion and gear are

$$m_1\ddot{y}_1 = F_k + F_c - F_u - F_{uc},$$

$$m_2\ddot{y}_2 = F_k + F_c - F_l - F_{lc}. \tag{16}$$

The rotary motion equations of the pinion and gear are

$$I_1\ddot{\theta}_1 = M_{pk} + M_{pc} - R_{b1}(F_k + F_c),$$

$$I_2\ddot{\theta}_2 = R_{b2}(F_k + F_c) - M_{gk} - M_{gc}. \tag{17}$$

The rotary motion equations of the motor and load are:

$$I_m\ddot{\theta}_m = M_1 - M_{pk} - M_{pc},$$

$$I_b\ddot{\theta}_b = -M_2 + M_{gk} + M_{gc}. \tag{18}$$

The values of forces and moments are given by

$$F_k = k_t(R_{b1}\theta_1 - R_{b2}\theta_2 - y_1 + y_2),$$

$$F_c = c_t(R_{b1}\dot{\theta}_1 - R_{b2}\dot{\theta}_2 - \dot{y}_1 + \dot{y}_2), \tag{19}$$

$$F_u = k_1 y_1,$$

$$F_{uc} = c_1\dot{y}_1,$$

$$F_l = k_2 y_2,$$

$$F_{lc} = c_2\dot{y}_2, \tag{20}$$

$$M_{pk} = k_p(\theta_m - \theta_1),$$

$$M_{pc} = c_p(\dot{\theta}_m - \dot{\theta}_1),$$

$$M_{gk} = k_g(\theta_2 - \theta_b),$$

$$M_{gc} = c_g(\dot{\theta}_2 - \dot{\theta}_b). \tag{21}$$

With the established model, the next step is to use these sets of equations for computer simulation when the gear is new or cracked to various degrees. To focus on the effects of crack size thorough the total mesh stiffness, we have further assumed that the vertical radial stiffness of the input bearings, k_1, and that of the output bearings, k_2, are identical and constant, that is, $k_1 = k_2 = k_r$; the damping coefficient of the input bearings, c_1, and that of the output bearings, c_2, are equal to a constant c_r; the torsional stiffness of the input flexible coupling, k_p, and that of the output flexible coupling, k_g, are equal to a constant k_c; the damping coefficient of the input flexible coupling, c_p, and that of the output flexible coupling, c_g, are equal to c_c. Also, the mesh damping coefficient, c_t, is set to be proportional to the total mesh stiffness, k_t, that is,

$$c_t = \mu k_t, \tag{22}$$

where μ is the scale constant measured in seconds, and its value has been selected in this simulation as $3.99 \times 10^{-6}(s)$. Furthermore, the other parameters of the gearbox system are listed in Table 3. Using Matlab's ODE15s function, the displacement plots can be derived for the perfect gear teeth and cracked gear tooth with increasing deterioration levels.

As described before, the crack length grows from zero with an increment size of 0.1 mm. This incremental crack size is expressed as a percentage of the theoretical through-tooth crack size and is approximately 1% (= 0.1 mm/7.8 mm). Since the tooth may suffer a sudden breakage before the crack develops to its full length, the maximum crack level is assumed to be 80%. Fig. 9 shows the dynamic response of the meshing gears when the crack levels are 0%, 2%, 6%, 18%, and 28%, respectively. Fig. 10 provides the dynamic response when the crack levels are 42%, 53%, 71%, and 78%, respectively.

In Fig. 9, the fault influences are not very obvious to visual observation; the signals look very similar compared to the perfect gear vibration signal (0% crack). The vibration signals generated with crack levels lower than 30% look quite similar to one another. As shown in Fig. 10, tooth root crack of levels higher than 40% produces obvious changes in the gear vibration signals. The obvious periodical impulses caused by the cracked tooth appear in the time domain signal as the crack level increases; this carries diagnostic information

Table 3
Main parameters of the gearbox system [4]

Mass of the pinion	$m_1 = 0.96\,\text{kg}$
Mass of the gear	$m_2 = 2.88\,\text{kg}$
Contact ratio	$C_r = 1.6456$
Mass moment of inertia of the motor	$I_m = 0.0021\,\text{kg m}^2$
Mass moment of inertia of the load	$I_b = 0.0105\,\text{kg m}^2$
Mass moment of inertia of the pinion	$I_1 = 4.3659 \times 10^{-4}\,\text{kg m}^2$
Mass moment of inertia of the gear	$I_2 = 8.3602 \times 10^{-3}\,\text{kg m}^2$
Input shaft frequency	$f_1 = 30\,\text{Hz}$
Mesh frequency	$f_m = 570\,\text{Hz}$
Input motor torque	$M_1 = 11.9\,\text{N m}$
Output load torque	$M_2 = 48.8\,\text{N m}$
Torsional stiffness of the coupling	$k_c = 4.4 \times 10^4\,\text{N m/rad}$
Damping coefficient of the coupling	$c_c = 5.0 \times 10^5\,\text{N m/rad}$
Radial stiffness of the bearing	$k_r = 6.56 \times 10^7\,\text{N/m}$
Damping coefficient of the bearing	$c_r = 1.8 \times 10^5\,\text{N s/m}$

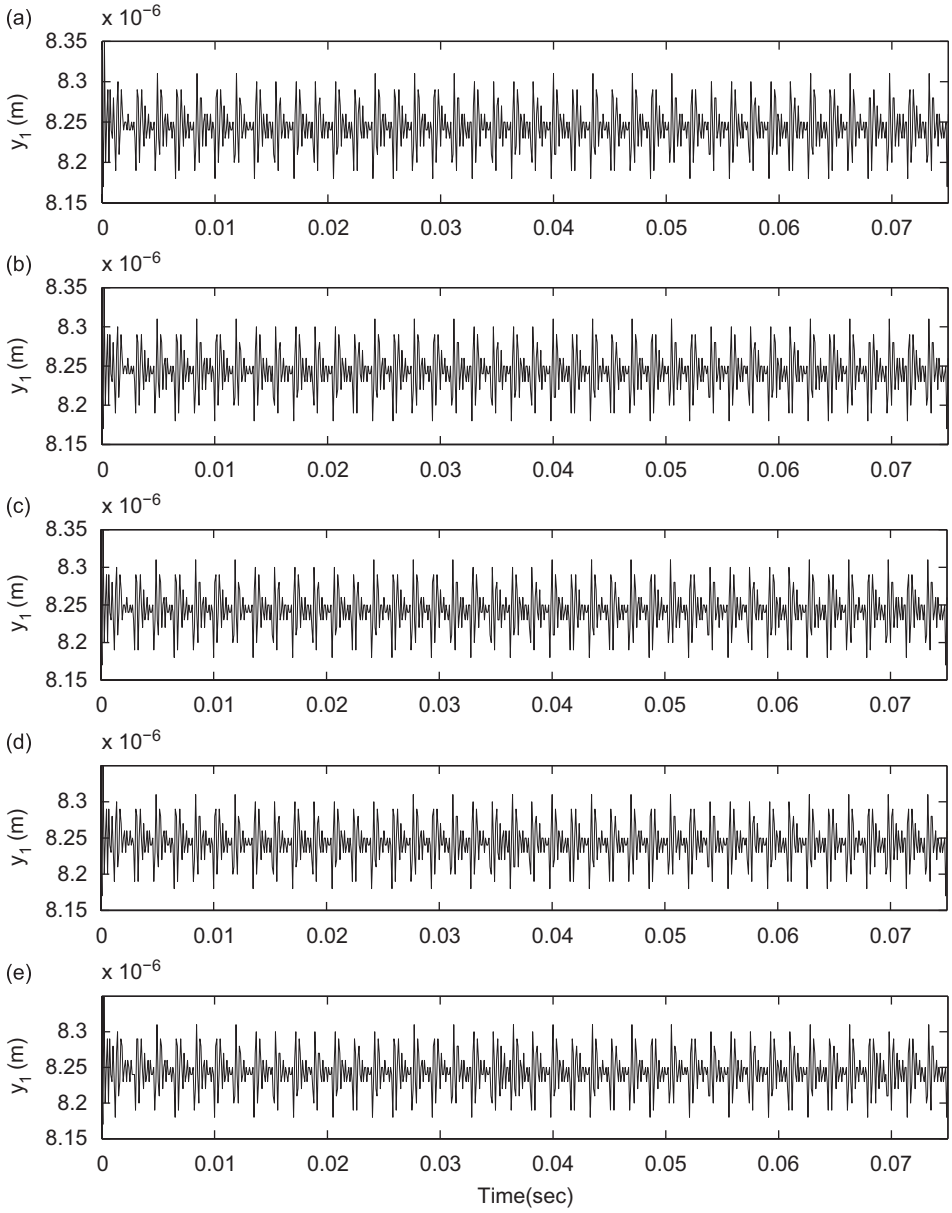

Fig. 9. The pinion's vibration displacement response in the y direction for a cracked gear tooth with different crack levels: (a) tooth with 0% crack, (b) tooth with 2% crack, (c) tooth with 6% crack, (d) tooth with 18% crack, (e) tooth with 28% crack.

that is important for extracting features of tooth defects. Because the influence caused by the cracked tooth repeats only once in a revolution, the duration between every two impulses is equal to one shaft period ($T_1 = 1/f_1 = 0.033$ s). The visually observable signs of the crack when the crack size are very large (more than 50%, say) has no practical usefulness. The tooth would have broken off when the crack is this large since most gearboxes work under heavy load. But, the simulated vibration responses under various sizes of crack enable us to compare the performance of different signal processing techniques and different fault growth indicators. We are interested in those indicators that are able to reflect the presence of crack that is as small as possible, say 10% or 15%. In the following sections, we examine several signal processing and statistical techniques for early crack detection.

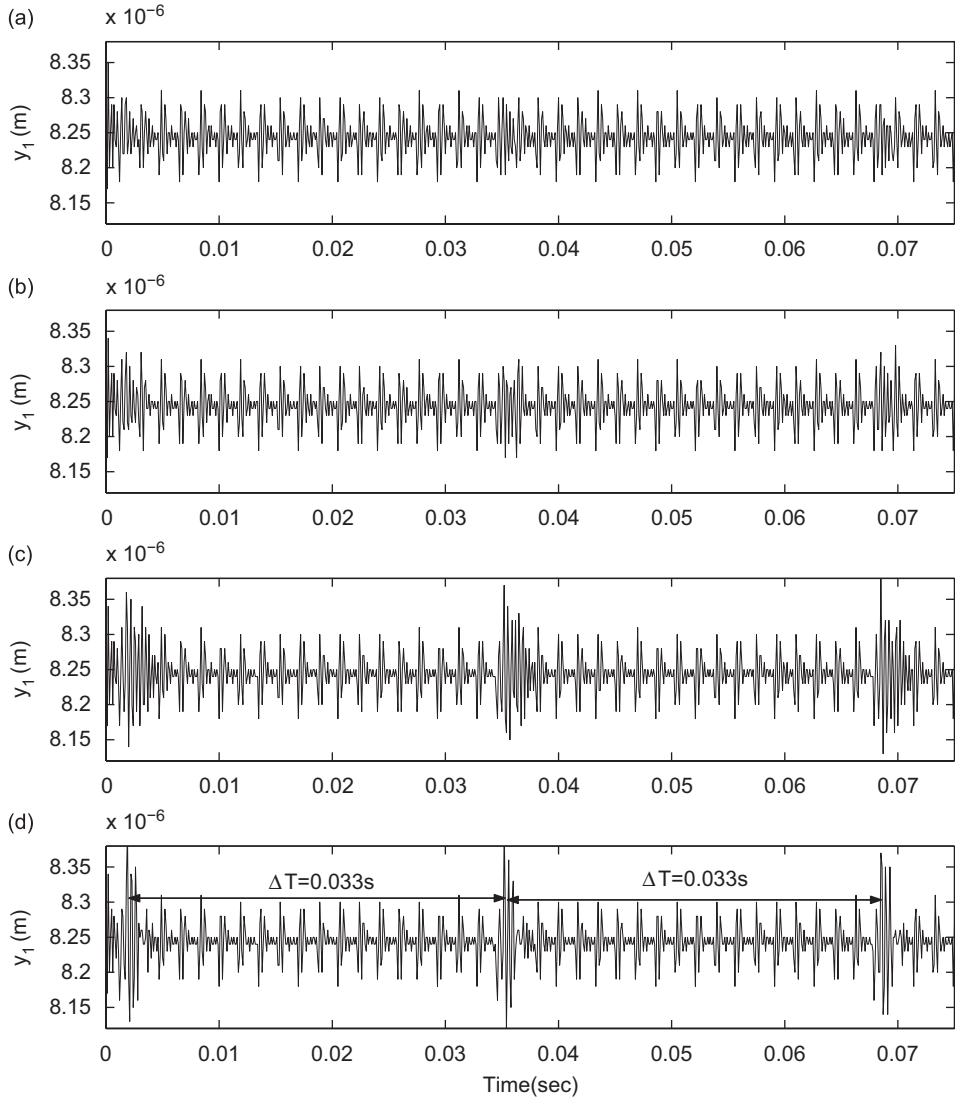

Fig. 10. The pinion's vibration displacement response in the y direction for a cracked gear tooth: (a) tooth with 42% crack, (b) tooth with 53% crack, (c) tooth with 71% crack, (d) tooth with 78% crack.

4. Estimation of crack growth using statistical techniques

Since the vibration signals at different tooth crack levels have been simulated, we would like to evaluate different statistical indicators for effective indication of tooth crack growth. Indicators using three different types of signals derived from the simulated vibration signals will be examined.

4.1. Original signals

A number of simple signal metrics based on the time domain waveform still have widespread applications in mechanical fault detection, the simplest of these being the rms value of the signal which is used for overall vibration level measurements [22]. rms is a kind of average of the signal; for discrete signals, the rms value is

defined as [22]

$$\text{rms} = \sqrt{\frac{1}{N}\sum_{n=1}^{N}(x(n)-\bar{x})^2},$$

$$\bar{x} = \frac{1}{N}\sum_{n=1}^{N}x(n), \tag{23}$$

where N is the number of data points taken in the signal, $x(n)$ is the amplitude of the signal of the nth point, and $\bar{x}$ is the mean value of all the amplitudes.

In the past few years, higher order statistics have been generating intensive interest. Kurtosis is a parameter that is sensitive to the shape of the signal and is well adapted to the impulse nature of the stimulating forces generated by component damage [23]. Its value can be given by [23]

$$\text{kurtosis} = \frac{(1/N)\sum_{n=1}^{N}(x(n)-\bar{x})^4}{[(1/N)\sum_{n=1}^{N}(x(n)-\bar{x})^2]^2}. \tag{24}$$

Similar to kurtosis, a third statistical moment parameter, S_r, was developed in Ref. [24]. It was found to have the same traditional merit as kurtosis, and it was less sensitive to spurious vibrations and more stable under different loads and speeds. The equation for S_r is given as follows [25]:

$$S_r = \frac{(1/N)\sum_{n=1}^{N}[(x(n)-\bar{x})^2]^{3/2}}{[(1/N)\sum_{n=1}^{N}(x(n)-\bar{x})^2]^{3/2}}. \tag{25}$$

Based on the comments given in Ref. [25], both kurtosis and S_r had their own advantages and disadvantages. Thus, a new statistical moment, S_α was proposed in Ref. [25]; it was shown to have lower susceptibility to spurious vibrations than kurtosis and higher sensitivity to impulse signals than S_r. It is defined as [25]

$$S_\alpha = \frac{(1/N)\sum_{n=1}^{N}|x(n)-\bar{x}|^3}{(1/N)\sum_{n=1}^{N}|x(n)-\bar{x}|)^3}, \tag{26}$$

Fault growth parameter (FGP) was another newly proposed indicator and its revised version FGP1 was provided by Lin et al. [12]. Their definitions are given below:

$$\text{FGP} = 100\sum_{i=1}^{L}\frac{1}{L}I(r_i > \bar{r} + 3\sigma_0), \tag{27}$$

where r_i's are the current residual error signal points, $\bar{r}$ is the mean value of the signal, σ_0 is the baseline standard deviation, and $I(.)$ is a zero-one indicator function:

$$\text{FGP1} = 100\sum_{i=1}^{L}\frac{w_i}{W}I(r_i > \bar{r} + 3\sigma_0), \tag{28}$$

where

$$w_i = I(r_i \leqslant \bar{r} + 3\sigma_0) + \left(\left\lfloor \frac{r_1 - \bar{r}}{3\sigma_0} - 1 \right\rfloor + 1\right),$$

$$W = \sum_{i=1}^{L} w_i$$

and $\lfloor . \rfloor$ is the floor function.

We have calculated the indicators defined above directly from our simulated vibration signals. We get a value for each indicator at each crack level. Our purpose is to find out which indicator is the most effective in reflection of the crack growth level. Since the values of FGP and FGP1 represent the outlier percentage of the signal values compared to the healthy tooth vibration signal, and the other indicators only show the actual

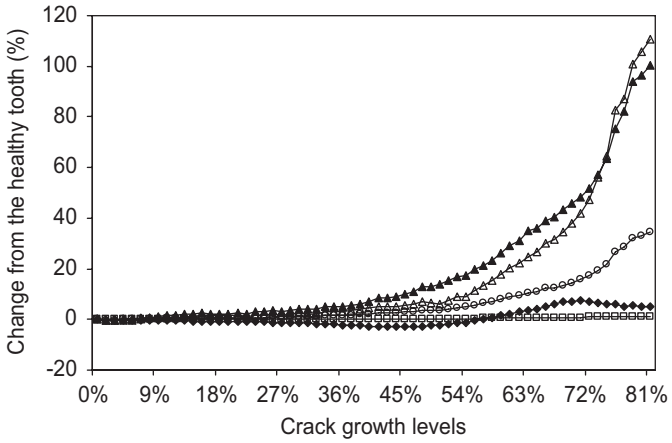

Fig. 11. Comparison among S_α, S_r, kurtosis, rms, FGP, and FGP1; ▲: S_α, ○: S_r, △: kurtosis, ◆: rms, □: FGP and FGP1.

values of the cracked tooth vibration signals; to make them comparable, we express all indicators as a percentage of change from the healthy condition. Let us use kurtosis as an example. We deduct the healthy tooth signal kurtosis from the cracked tooth signal kurtosis, divide the difference by the healthy tooth signal kurtosis, and express the result in the form of a percentage. This value shows the change of cracked tooth signal kurtosis from the healthy tooth kurtosis. Repeat the same procedure for rms, S_α, and S_r, and the calculation results are shown in Fig. 11.

From Fig. 11, we can observe that FGP and FGP1 are virtually not responsive to crack growth at all. rms fluctuates around the x-axis and is slightly above 0 when the crack level is at its maximum (80%). It is apparent that none of these three indicators provide any useful indication of the growth in the tooth crack. On the other hand, both kurtosis and S_α exhibit a similar and obvious increasing trend when the crack level becomes higher than 40%. When the crack level reaches 60%, both show sharp increases. This means that kurtosis and S_α are effective indicators of crack tooth damage when the level of damage reaches around 40–60%. The performance of the last indicator, S_r , is right in the middle, neither the best and nor the worst. Our conclusion is then, when the original signals are used directly, kurtosis and S_α are found to be the better indicators of crack growth when the damage level reaches 40%. The other three indicators do not work as well.

4.2. Residual signals

The idea of residual signal was first proposed by Stewart [26] in 1977. For healthy gears, the gear meshing frequency and its harmonics and the shaft rotation frequencies and their harmonics, which constitute the so-called regular signals, dominate the meshing vibration spectrum [27]. When a local gear fault such as a crack in a tooth is present, the vibration signal in a complete revolution will be modified by the effects of a short duration impact impulse, and thus the regular components of the signal are actually redundant for the purpose of fault detection. Thus, in order to effectively detect the fault features in the vibration signal, the regular components need to be removed; the rest is called the residual signal, which is supposed to be more sensitive to crack growth.

In two separate subsections, we will examine two different methods of generating residual signals. The indicators calculated based on these two different methods will be checked for effective indication of crack growth. The first method is based on the literal definition of the residual signal given in Ref. [26], and the other one is proposed in this paper.

4.2.1. Method 1 of generating residual signals

Based on the definition of residual signal given in Ref. [26], after removing gear meshing frequency and shaft frequency and their harmonics, residual signals of simulated vibration signals have been obtained. The same

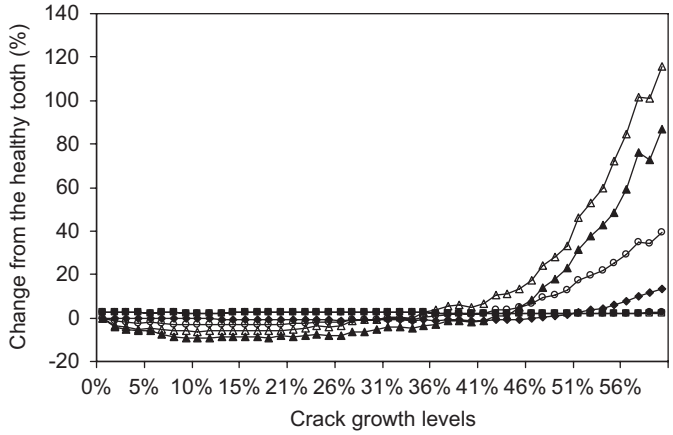

Fig. 12. Comparison among S_α, S_r, rms, kurtosis, FGP, and FGP1 using Method 1; ▲: S_α, ○: S_r, △: kurtosis, ◆: rms, □: FGP, ●: FGP1.

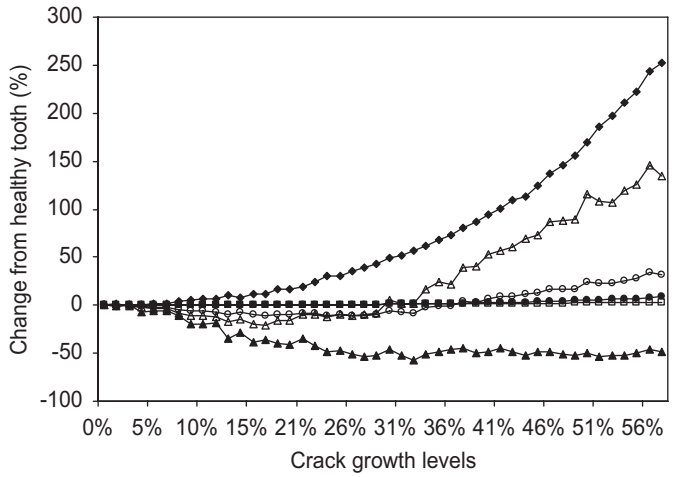

Fig. 13. Comparison among S_α, S_r, rms, kurtosis, FGP, and FGP1 using Method 2; ▲: S_α, ○: S_r, △: kurtosis, ◆: rms, □: FGP, ●: FGP1.

set of indicators are used here and their values as a function of the crack level are plotted in Fig. 12. From Fig. 12, it can be seen that trends of these indicators are similar to those shown in Fig. 11. The relative merits of these indicators are identical too. FGP, FPG1, and rms perform the worst, S_r is in the middle, and again kurtosis and S_α are the best. Both kurtosis and S_α show obvious increasing trends only when the crack level has reached 40%. It can be concluded that there is no advantage of using residual signals generated with Method 1. One can get results of similar value when the original signals are used directly.

4.2.2. Method 2 of generating residual signals

We now consider another method of deriving the residual signal. The objective of getting the residual signal is to remove the influence of the regular vibration components and highlight the signal components generated by crack damage. When there is no crack in any of the gears, the obtained vibration signal can be considered to be the regular signals. Thus, if we select the vibration signal with 0% crack as a reference signal, and remove it from each set of cracked gear vibration signals, the information contained in the remaining part is supposed to be only related to the gear faults. Then, we apply the aforementioned indicators to the residual signal obtained from Method 2 and their values as a function of the crack level are shown in Fig. 13.

As can be observed from Fig. 13, unlike the results obtained from the original signals and the residual signals based on Method 1, rms stands out to be the best indicator of crack growth, kurtosis ranks as the

second best, S_α becomes one of the worst, FGP, FGP1, and S_r are still pretty bad. rms shows obvious increasing pattern when the crack level is as early as 20%. Kurtosis also exhibits earlier sharp increases when the crack level reaches 35%. Both of these two indicators can be considered to be effective indicators of early crack growth.

With tooth crack growing, the values of S_α keep decreasing rather than increasing; this makes it impossible to indicate crack growth. A mathematical explanation for such a phenomenon is that the denominator of the S_α formula increases faster than the numerator. Though the amplitude of several signal samples, $x(n)$, are enhanced due to the appearance of tooth damage, the values of S_α are still reduced.

An explanation for rms's excellent performance is that using the second method of generating residual signals, the healthy tooth signal is totally removed, and there is no noise in the pure simulation signal, the remaining parts must be all caused by gear crack damage. Thus, the periodical magnitudes are strong enough to enhance the total signal average. This exactly matches the features of rms, which is used to represent the signal's average amplitude level. Therefore, rms becomes the most sensitive one in this set of test.

After comparing all these statistical indicators using original signals and residual signals generated with two different methods, we can see that kurtosis emerges to be the most robust crack indicator no matter what signals are used. If we use the second method of generating residual signals, rms is the best indicator to use. We note that to apply Method 2 of generating residual signals, we need to collect a reference signal of the shaft rotation so that the starting point of collecting healthy gearbox signals is the same as that of collecting deteriorated gearbox signals.

5. Conclusions and future work

This paper studies through computer simulation the effects of tooth crack growth on the vibration response of a one-stage gearbox with spur gears. A pair of meshing spur gears consisting of a perfect gear and a pinion with a cracked tooth has been analyzed. The pinion is simulated with crack levels varying from 0% to 80% of the tooth root thickness. An analytic model for calculating total mesh stiffness with a gear tooth cracked at different levels is developed. The numeric values of the calculated total mesh stiffness are input into a lumped parameter model to simulate the vibration response of the pair of meshing gears under different deterioration levels of the tooth crack on the pinion. The simulated vibration signals are analyzed directly and also through two different methods of generating residual signals. Several statistical indicators are evaluated to reflect the crack growth in the simulated vibration signals. It has been found that rms performs the best when Method 2 of generating residual signals is used and kurtosis is the most robust indicator no matter what signals are used. Future research topics include crack initiation points, more realistic crack propagation path, manufacturing errors in gears, friction in meshing, noise in vibration response, and evaluation of various fault growth indicators using laboratory vibration signals and field vibration signals.

Acknowledgments

This research was supported by the Natural Sciences and Engineering Research Council of Canada (NSERC). Comments and suggestions from anonymous referees and editors are very valuable in the improvement of the quality of this paper.

References

[1] S.J. Loutridis, Instantaneous energy density as a feature for gear fault detection, *Mechanical Systems and Signal Processing* 20 (5) (2006) 1239–1253.

[2] R. Kasuba, J.W. Evans, An extended model for determining dynamic loads in spur gearing, *Journal of Mechanical Design, Transactions of the American Society of Mechanical Engineers* 103 (2) (1981) 398–409.

[3] D.C.H. Yang, J.Y. Lin, Hertzian damping, tooth friction and bending elasticity in gear impact dynamics, *Journal of Mechanisms, Transmissions, and Automation in Design* 109 (2) (1987) 189–196.

[4] X.H. Tian, Dynamic Simulation for System Response of Gearbox including Localized Gear Faults, Master's Thesis. University of Alberta, Edmonton, Alberta, Canada, 2004.

[5] W. Bartelmus, Mathematical modelling and computer simulations as an aid to gearbox diagnostics, *Mechanical Systems and Signal Processing* 15 (5) (2001) 855–871.
[6] V.K. Tamminana, A. Kahraman, S. Vijayakar, A study of the relationship between the dynamic factors and the dynamic transmission error of spur gear pairs, *Journal of Mechanical Design* 129 (2007) 75–84.
[7] L. Vedmar, A. Andersson, A method to determine dynamic loads on spur gear teeth and on bearings, *Journal of Sound and Vibration* 267 (2003) 1065–1084.
[8] V. Kartik, D.R. Houser, Analytical predictions for the transmission error excitation in various multiple-mesh gear-trains, *Proceedings of the 2003 ASME Design Engineering Technical Conferences and Computers and Information in Engineering Conference, Vol. 4: Ninth International Power Transmission and Gearing Conference*, 2003, pp. 515–524.
[9] P. Velex, M. Ajmi, Dynamic tooth loads and quasi-static transmission errors in helical gears—approximate dynamic factor formulae, *Mechanism and Machine Theory* 42 (2007) 1512–1526.
[10] S. He, R. Gunda, R. Singh, Effect of sliding friction on the dynamics of spur gear pair with realistic time-varying stiffness, *Journal of Sound and Vibration* 301 (3–5) (2007) 927–949.
[11] V.B. Rao, Kurtosis as a metric in the assessment of gear damage, *Mechanical Systems and Signal Processing* 31 (6) (1999) 443–448.
[12] D. Lin, M. Wiseman, D. Banjevic, A.K.S. Jardine, An approach to signal processing and condition-based maintenance for gearboxes subject to tooth failure, *Mechanical Systems and Signal Processing* 18 (5) (2004) 993–1007.
[13] S.Y. Wu, Gearbox Dynamic Simulation and Estimation of Fault Growth, Master's Thesis, Department of Mechanical Engineering, University of Alberta, Edmonton, Alberta, 2007.
[14] S.Y. Wu, M.J. Zuo, Gearbox dynamic simulation and estimation of fault growth, *Proceedings of the Second World Congress on Engineering Asset Management and the Fourth International Conference on Condition Monitoring*, Harrogate, UK, 11–14 June, 2007.
[15] X.H. Tian, M.J. Zuo and K.R. Fyfe, Analysis of the vibration response of a gearbox with gear tooth faults, *Proceedings of IMECE04, 2004 ASME International Mechanical Engineering Congress and Exposition*, November 13–20, 2004, Anaheim, CA, USA.
[16] N. Baydar, A. Ball, Detection of gear failures via vibration and acoustic signals using wavelet transform, *Mechanical Systems and Signal Processing* 17 (4) (2003) 787–804.
[17] W.X. Lai, P.W. Tse, G.C. Zhang, T.L. Shi, Classification of gear faults using cumulants and the radial basis function network, *Mechanical Systems and Signal Processing* 18 (2) (2004) 381–389.
[18] G. Meltzer, N.P. Dien, Fault diagnosis in gears operating under non-stationary rotational speed using polar wavelet amplitude maps, *Mechanical Systems and Signal Processing* 18 (5) (2004) 985–992.
[19] I. Yesilyurt, F.S. Gu, A.D. Ball, Gear tooth stiffness reduction measurement using modal analysis and its use in wear fault severity assessment of spur gears, *NDT and E International* 36 (5) (2003) 357–372.
[20] J. Kramberger, M. Sraml, S. Glodez, J. Flasker, I. Potrc, Computational model for the analysis of bending fatigue in gears, *Computers and Structures* 82 (23–26) (2004) 2261–2269.
[21] D.G. Lewicki, Gear crack propagation path studies—guidelines for ultrasafe design, *Journal of the American Helicopter Society* 47 (1) (2002) 64–72.
[22] B.D. Forrester, Advanced Vibration Analysis Techniques for Fault Detection and Diagnosis in Geared Transmission Systems, PhD Thesis, Swinburne University of Technology, 1996.
[23] J.P. Dron, F. Bolaers, I. Rasolofondraibe, Improvement of the sensitivity of the scalar indicators (crest factor, kurtosis) using a de-noising method by spectral substraction: application to the detection of defects in ball bearings, *Journal of Sound and Vibration* 270 (1–2) (2004) 61–73.
[24] F. Honarvar, H.R. Marin, New statistical moments for diagnostics of rolling element bearings, *Journal of Manufacturing Science and Engineering* 119 (1997) 425–432.
[25] B. Tao, L.M. Zhu, H. Ding, Y.L. Xiong, An alternative diagnostic index of rolling element bearings—a comparison study, *Reliability Engineering and System Safety* 92 (5) (2007) 660–670.
[26] R.M. Stewart, Some Useful Data Analysis Techniques for Gearbox Diagnostics. Applications of Time Series Analysis, PhD Thesis, ISVR, University of Southampton, 1977.
[27] W.Y. Wang, Early detection of gear tooth cracking using the resonance demodulation technique, *Mechanical Systems and Signal Processing* 15 (5) (2001) 887–903.